Efficient mass conservative numerical model for solving variably saturated groundwater flow

Abdelkrim Aharmouch, Brahim Amaziane

Efficient Mass Conservative Numerical Model for Solving Variably Saturated Groundwater Flow

Abdelkrim Aharmouch[a] and Brahim Amaziane[b*]

[a]Université Sidi Mohamed ben Abdellah, Faculté des Sciences (Dhar Mahraz).
Laboratoire d'Informatique, Signaux, Automatique et Cognitivisme (LISAC)
P. O. Box 1796, Fès-Atlas 30003, Fès, Morocco Abdelkrim.aharmouch@usmba.ac.ma

[b]Universite de Pau et des Pays de l'Adour, E2S UPPA, CNRS, LMAP, Pau, France
brahim.amaziane@univ-pau.fr

Summary

A multi-dimensional mass conservative numerical method, particularly suitable for limited computational resources, is developed for solving transient variably saturated groundwater flow problems. The Richards equation is discretized spatially with a finite element method and temporally with an implicit Euler scheme, in which mass-conservative and mass-lumping techniques are used to keep the numerical simulation stable. In addition, the stiffness and mass matrices involved are approximated in a way to guarantee less computational effort. To confirm the accuracy and the efficiency of this code, we verified it using benchmark tests using one, two and three-dimensional problems. The present model is also applied to a real field case problem, where its superiority is clearly demonstrated. The code achieved reliable results for each problem.

Keywords

Groundwater Flow, Finite Element, Modeling, Richards Equation, Variably Saturated Flow

E-mail address : brahim.amaziane@univ-pau.fr (B. Amaziane)

1 Introduction

Flow in a variably saturated porous medium is governed by the Richards equation, a highly nonlinear PDE. Few analytical solutions using simplifying conditions or restrictive hypotheses were presented (Polubarinova, 1962; Teloglou et al, 2008; Moutsopoulos, 2013; Tracy, 1995, 2006, 2007; Hayek, 2015). Nevertheless, the most attempts to solve saturated-unsaturated flow problems are based on numerical techniques.

Several models, using the numerical approach of Celia et al. (1990), were developed (Clement et al, 1994; Van dam and Feddes, 2000; Kuznetsov et al, 2012; Herada, 2014). Belfort et al. (2013) presented a review of several estimations of the equivalent conductivity and analyzed the efficiency of the different averaging fashions when solving unsaturated flow. Fahs et al (2009) used the method of lines combined with the mixed finite element discretization to solve variably saturated flow in porous media. Younes et al (2013) studied the monotonicity of a finite volume-based method for solving flow in variably saturated and heterogeneous porous media. Hassane Maina and Ackerer (2017) discussed Newton-Raphson method and time-stepping strategies for solving the mixed form of Richards equation. Koohbor et al (2020) solved Richards equation in the context of fractured porous media. Zha et al. (2017) presented a modified Picard iteration scheme for overcoming drawbacks arising when simulating infiltration into dry soils. Farthing and Ogden (2018) and Zha et al (2019) presented a state-of-the-art review of the numerical solution of the Richards equation. Numerous aspects were discussed and challenges underlined related to equivalent hydraulic conductivity, computational efficiency or choice of primary variable among others.

Other models were also developed (Thoms et al, 2006; Šimůnek et al, 2006) in view to solve 3D flow in variably saturated porous media. These numerical models proceed by solving the resulting equations system subsequent to various approximation methods. However, these codes may be costing in CPU time when much finer temporal and spatial discretizations are

necessary, or in case of applications at the watershed scale, e. g., for climate change purposes when huge equations systems are to be solved. Drawbacks to the numerical resolution attempt of the Richards equation may be exacerbated, when computational resources are limited. Alternatives are proposed to avoid high CPU time costs of fully 3D numerical modes (Yakirevich et al, 1998; Paulus et al, 2013; Kuznetsov et al, 2012; Xu et al, 2012). These techniques act by lowering dimensions of the fully 3D Richards equation in both unsaturated and saturated domains or only in the unsaturated one when the saturated flow is modeled in its whole dimensionality. As a consequence the number of unknowns to be solved decrease significantly and the CPU time as well. However, doing so may constitute a source of inaccuracies that can affect the hydraulic heads as well as the fluxes in the separated domains. Indeed, as it is pointed out by Twarakavi et al. (2008), only solving the fully 3D Richards equation for the whole continuous flow domain is able to provide accurate solutions for hydraulic heads and subsequent fluxes in both unsaturated and saturated compartments. However, the most obstacle that limits the applicability of such models for regional scales is their computational demand and time cost.

In this paper, a multi-dimensional numerical model based on the mixed form of Richards equation, particularly suitable for limited computational resources, is developed to solve flow equation in both unsaturated and saturated zones under unsteady and steady regimes. The numerical model is Galerkin FE based and uses the Celia et al's (1990) first-order time integration method to solve the derived algebraic equations system. The use the Richrads equation may be inappropriate with coarse grids because of violation of the assumption of representative elementary volume which can result in loss of accuracy (Zha et al, 2019). The use of the fine grids, however, may complicate the resolution or simply make it infeasible due to high computational coast. In order to circumvent these difficulties, the proposed numerical

numerical scheme approximates the matrices involved in a newly fashion to guarantee less computational effort, when solving the involved PDE.

The paper is organized as follows: section 2 describes the flow model used to solve variably saturated porous media and reports the most used retention curves equations. Section 3 is dedicated to the numerical procedure adopted and the proposed approximation of the matrices obtained. In section 4 benchmark tests against analytical solutions show the present model capabilities to provide high level of accuracy. In addition, other tests available in the literature are also examined and the efficiency of the present model is demonstrated. Finally, section 5 summarizes the concluding remarks.

2. Mathematical statement

The Richards equation can be expressed on three usual forms: the head-based form, the moisture-based form and under a mix form using the moisture and the head for the temporal and the spatial terms respectively. Discussion about these forms can be found in Fahs et al (2009), Farthing and Ogden (2018) and Zha et al (2019).

The mixed form of Richards' equation, modeling water flow in a variably saturated porous medium, is obtained by combining Darcy's law and continuity equation and is expressed as:

$$\nabla.\left(\mathbf{K}_{\mathrm{s}} K_r(h)\nabla h\right) - q = \frac{\partial \theta}{\partial t} \tag{1}$$

Where $\mathbf{K}_{\mathrm{s}}$ is the saturated hydraulic conductivity tensor, $K_r(h)$ is the relative conductivity, q is the source/sink per volume of aquifer, θ stands for the volumetric moisture content and h is the hydraulic head.

Solving Richards' equation necessitates eliminating one of the two dependent variables, water content and the pressure head $\psi = h - z$ (where z is elevation). This is often done by introducing constitutive equations, namely the water retention curves that express the water

content and the relative conductivity, as functions of the pressure head. Various formulations can be found in the literature. In this work some of them will be used ranging from simplest to very complex ones and are listed below.

Based on the model of Irmay (1954), the moisture content, as in Tracy (2006), is expressed as:

$$\theta = \begin{cases} \theta_r + (\theta_s - \theta_r) e^{\alpha\psi} & \psi < 0 \\ \theta_s & \psi \geq 0 \end{cases} \tag{2}$$

Where θ_s and θ_r are saturated and residual moisture content respectively.

Gardner (1958) expressed the relative conductivity as an exponential function of the pressure head:

$$k_r(\psi) = \begin{cases} e^{\alpha\psi} & \psi < 0 \\ 1 & \psi \geq 0 \end{cases} \tag{3}$$

The moisture content and the relative conductivity formulated by Van Genuchten (1980) are very popular and are written as:

$$\theta = \begin{cases} \dfrac{(\theta_s - \theta_r)}{\left(1 + (\alpha|\psi|)^n\right)^m} + \theta_r & \psi < 0 \\ \theta_s & \psi \geq 0 \end{cases} \tag{4}$$

$$k_r(\psi) = \begin{cases} \Theta^{\frac{1}{2}} \left(1 - \left(1 - \Theta^{\frac{1}{m}}\right)\right)^2 & \psi < 0 \\ 1 & \psi \geq 0 \end{cases} \tag{5}$$

Where $\Theta = \dfrac{\theta - \theta_r}{\theta_s - \theta_r}$ expresses the effective saturation and α, n and $m = \dfrac{n-1}{n}$ are constants depending upon the soil properties.

Brooks and Corey (1964) provided also equations describing hydraulic properties of soils, expressed originally as functions of the moisture content θ:

113 $$\psi = \psi_s \left(\frac{\theta - \theta_r}{\theta - \theta_s} \right)^{-\frac{1}{\lambda}} \quad (6)$$

114 $$k_r(\theta) = \left(\frac{\theta - \theta_r}{\theta - \theta_s} \right)^{\frac{2+3\lambda}{\lambda}} \quad (7)$$

115 Where $\psi_s = \psi(\theta_s)$, is the pressure head at saturation, θ_r is the residual water moisture
116 content and λ is a parameter describing the pore-size distribution index of the medium.

117 Other relationships, linking moisture content and relative conductivity to the pressure head,
118 are presented by Haverkamp et al. (1977):

119 $$\theta = \begin{cases} \dfrac{A(\theta_s - \theta_r)}{1 + (100|\psi|)^B} + \theta_r & \psi < 0 \\ \theta_s & \psi \geq 0 \end{cases} \quad (8)$$

120 $$k_r(\psi) = \begin{cases} \dfrac{C}{C + (100|\psi|)^D} & \psi < 0 \\ 1 & \psi \geq 0 \end{cases} \quad (9)$$

121 Where A, B, C and D are constants to be determined experimentally for the soil type.

122 # 3. Numerical solution

123 ## 3.1. Finite element model

124 To solve the flow equation (1), the finite element Galerkin method with linear basis functions
125 is used to discretize the whole domain of flow (saturated and unsaturated), along with an
126 implicit finite difference scheme for time. Linear, rectangular and hexahedral elements are
127 used in the codes for 1D, 2D and 3D features. Discretization leads to the following system of
128 nonlinear equations:

129 $$\mathbf{G}(\mathbf{h}^{k+1})\mathbf{h}^{k+1} + \mathbf{M}(\mathbf{h}^{k+1}) - \mathbf{q}(t^{k+1}) = 0 \quad (10)$$

where $\mathbf{h}^{k+1}$ is the vector of nodal head values at time t^{k+1}, k is a time step index. $\mathbf{G}$ is the conductance (stiffness) matrix, $\mathbf{M}$ is a vector containing the moisture content derivative with respect to time and $\mathbf{q}$ is a vector containing the boundary conditions and flow rates pumped or injected.

3.2. Linearization technique

Applied to (10), the Picard scheme, where the soil moisture at the current iteration level is approximated as a truncated expansion of Taylor series about the pressure head at the last iteration level (Celia et al, 1990), gives the following system of linear equations to be solved for $\mathbf{h}^{k+1,m+1}$, the vector of nodal hydraulic heads at the current iteration level; superscript m is the iteration index:

$$\mathbf{G}(\mathbf{h}^{k+1,m})\mathbf{h}^{k+1,m+1} + \mathbf{C}(\mathbf{h}^{k+1,m})\frac{\mathbf{h}^{k+1,m+1} - \mathbf{h}^{k+1,m}}{\Delta t^{k+1}} + \mathbf{M}(\mathbf{h}^{k+1,m}) - \mathbf{q}(t^{k+1}) = 0 \qquad (11)$$

Stiffness matrix $\mathbf{G}$, mass matrix $\mathbf{C}$ and vector $\mathbf{M}$ depend upon the hydraulic head.

The entries of these matrices and the elements of the vector are defined as follows:

$$G_{IJ} = \sum_e \int_{V^e} k_r{}^t \nabla b_i \mathbf{K_s} \nabla b_j dxdydz \qquad (12)$$

$$C_{IJ} = \sum_e \int_{V^e} S_g(\psi) b_i b_j dxdydz \qquad (13)$$

$$C_{II} = \sum_e \int_{V^e} S_g(\psi) b_i dxdydz \qquad (14)$$

Where $S_g(\psi) = \frac{\theta}{\theta_s} S_s + \frac{d\theta}{d\psi}$ indicates the general storage coefficient and S_s stands for the specific storage coefficient.

Equation (14) gives the coefficients of the mass matrix $\mathbf{C}$ if mass lumping technique is used.

149 $$M_I = \sum_e \int_{V^e} \frac{d\theta}{dt} b_i dxdydz \quad (15)$$

150 Chord slope is used to perform the moisture content derivative with respect to time as
151 follows:

152 $$\frac{d\theta}{dt} = \frac{\theta^{k+1,m} - \theta^k}{\Delta t^{k+1}} \quad (16)$$

153 *I* and *J* represent the global nodes, while b_i and b_j are basis functions related, respectively, to
154 local nodes *i* and *j* belonging to the element *e*. Gaussian quadrature rule is applied to perform
155 the integrals.

156 3.3. Solution procedure

157 To solve iteratively the equation (11), the matrices involved have to be updated at each
158 iteration level, making the solution process very costly on a CPU time basis, particularly for
159 large scale problems. To make the procedure fast, approximations are proposed for the matrix
160 coefficients (Aharmouch and Amaziane, 2012). The idea is to split the coefficients into to
161 quantities, one constant, computed once and stored, and the other varying with iteration,
162 needing to be updated. The authors applied the method to solve 3D steady state groundwater
163 flow problems only in the saturated zone and neglect the flow in the unsaturated region.
164 However, the flow modeling in the vadose zone constitutes an important issue in hydrology
165 and plays a key role for sustainable groundwater use, particularly in dry regions, by
166 evaluating the water transfer rates to the water table during recharge and also by assessing the
167 water losses during dry periods. For these purposes, retention curves equations have to be
168 used to characterize the unsaturated medium.

In the present work, the stiffness entries are approximated as in the work of Aharmouch and Amaziane (2012), but with incorporating the retention curves equations, aforementioned, to solve correctly the flow in the vadose zone as well as for the saturated one.

The stiffness entries (equation 12) are approximated for 1D, 2D and 3D features as:

$$G_{IJ} \cong k^* \sum_e \int_{-1}^{1} {}^t\nabla b_i \mathbf{K_s} b_j d\xi \tag{17}$$

$$G_{IJ} \cong k^* \sum_e \int_{-1}^{1}\int_{-1}^{1} {}^t\nabla b_i \mathbf{K_s} b_j d\xi d\eta \tag{18}$$

$$G_{IJ} \cong k^* \sum_e \int_{-1}^{1}\int_{-1}^{1}\int_{-1}^{1} {}^t\nabla b_i \mathbf{K_s} \nabla b_j d\xi d\eta d\zeta \tag{19}$$

$$k^* = \frac{1}{N_G . n_{eS}} \sum_{e=1}^{n_{eS}} \sum_{n_g=1}^{N_G} k_r\left(e, n_g\right).\det\left[\mathbf{J}\right]\left(e, n_g\right) \tag{20}$$

The mass matrix entries for the distributed form (equation 13) can be readily approximated as for the stiffness coefficients with making the necessary change. However, the lumped form (equation 14) is used only, because of its property to guarantee non oscillatory solution as it was demonstrated by Celia et al. (1990).

The mass matrix entries using mass lumping technique (equation 14) are approximated for 1D, 2D and 3D features as:

$$C_{II} \cong S_g^* \sum_e \int_{-1}^{1} b_i d\xi \tag{21}$$

$$C_{II} \cong S_g^* \sum_e \int_{-1}^{1}\int_{-1}^{1} b_i d\xi d\eta \tag{22}$$

$$C_{II} \cong S_g^* \sum_e \int_{-1}^{1}\int_{-1}^{1}\int_{-1}^{1} b_i d\xi d\eta d\zeta \tag{23}$$

$$S_g^{*} = \frac{1}{N_G . n_{eS}} \sum_{e=1}^{n_{eS}} \sum_{n_g=1}^{N_G} S_g\left(e, n_g\right).\det\left[\mathbf{J}\right]\left(e, n_g\right) \quad (24)$$

ξ, η and ζ are local coordinates, n_{eS} is the number of elements sharing the nodes *I* and *J*, n_g indicates Gauss integration points, $N_G\left(=2,4,8\right)$ stands for their numbers, depending on the dimensionality of the problem and $\det\left[\mathrm{J}\right](e, n_g)$ is the Jacobian matrix determinant related to Gauss integration point n_g and element *e*.

As it was pointed out in the work of Aharmouch and Amaziane (2012), k^{*} expresses the arithmetic mean of the term $k_r.\det[\mathrm{J}]$ over the integration points involved in the elements that share the nodes *I* and *J*. Similarly, it can be seen that S_g^{*} is the arithmetic mean of the term $S_g.\det[\mathrm{J}]$ over the integration points involved in the elements that share the nodes *I* and *J*. Only the hydraulic properties (relative conductivity and general storage coefficient) have to be updated during the iteration process, which guarantees gain in CPU time.

Time stepping is performed as in the work of Paniconi and Putti (1994). Time step sizes during transient simulations are dynamically recalculated depending on the convergence behavior of the nonlinear procedure. The simulations start with a certain time step Δt_0 which can be augmented, by a magnificence factor Δ_{mag}, to a certain Δt_{max}, or reduced, using a reduction coefficient Δ_{red} to a minimum value, Δt_{min} , depending on the number of iterations allowed in each nonlinear iteration and according to some performance criteria. If the convergence is achieved in less than $maxit_1$ iterations, the time step in increased and remains unchanged if the number of iterations is within $maxit_1$ and $maxit_2$ iterations and reduced if convergence iterations needed are more than $maxit_2$. The solution can also be recomputed at the current time, if convergence is not accomplished among the specified criteria, when maxit limit is exceeded, by reducing the time step and going back to the old status ("back stepping").

209 The infinity norm (l_∞) of the convergence error is adopted as stopping criterion of the
210 nonlinear iterative process, thus the convergence is achieved when $\left\|\mathbf{h}^{k+1,m+1}-\mathbf{h}^{k+1,m}\right\|_\infty < tol$ is
211 satisfied. In the field case example, the convergence is checked using a relative norm based
212 stopping criterion. The convergence is, therefore, achieved when $\frac{\left\|\mathbf{h}^{k+1,m+1}-\mathbf{h}^{k+1,m}\right\|_2}{\left\|\mathbf{h}^{k+1,m}\right\|_2} < tol$ is
213 satisfied, where $\|\cdot\|_2$ expresses the (l_2) norm (the square root of the sum of squares of a vector
214 components).

215 Owing to that the systems of linear equations obtained with the Picard finite element
216 approximation are sparse and symmetric, conjugate gradient solvers are particularly indicated
217 in such situation. In this work preconditioned conjugate gradient method with incomplete
218 Cholesky decomposition preconditioner (ICCG) is used to solve the resulting linear systems
219 for 2D and 3D problems, whereas tridiagonal direct algorithm is used for solving those
220 obtained for 1D configuration.

221 4. Numerical tests and model assessment

222 For validation purposes, numerical examples are treated to verify the proposed model
223 described in section 3 either (equations17—24), designated as "M_1" or equations (14 and
224 17—20), designated as "M_2". The obtained results are then checked against some available
225 solutions measured or analytical to account for the model accuracy. Numerous examples are
226 considered including 1D, 2D and 3D flow features and dealing with the most encountered
227 problems of groundwater in variably saturated porous media, ranging from infiltration-
228 evaporation in a soil column, recharge-drainage of a free surface 2D aquifer and free surface
229 3D aquifer response to recharge and pumping. Special attention is paid to flow in unsaturated
230 flow in porous media.

231 The efficiency of the proposed numerical model is demonstrated against the standard model,
232 labeled "Stand", where stiffness and mass matrices entries are expressed normally (equations
233 12 and 14).

234 Comparisons between the two models were focused on the following criteria:

235 — The number of time steps, Nts,
236 — The number of back steps, Nbs
237 — The total computation time, CPU,
238 — The total number of nonlinear iterations, Nnlit,
239 — The mass balance error, MBE, computed as in Yeh (1981).

240 All the simulations were performed on a 3.00 GHz Pentium Dual-Core E5700
241 microcomputer.

242 4.1. Transient flow in a soil column under infiltration

243 4.1.1. Description

244 This example was chosen to verify the presented model when dealing with infiltration. The
245 experimental results have been reported by Haverkamp et al. (1977). Later, Clement et al.
246 (1994) presented a 2-dimensional numerical study of the same case and checked the obtained
247 results to those observed by Haverkamp et al. (1977). In the present study, the flow domain is
248 a one-dimensional sand column of 0.7 m length, where a constant pressure head of ψ = -0.615
249 m is specified at the outlet and a constant flux of 3.29 m/day is imposed at the inlet.

250 The soil properties are taken as in Clement et al. (1994). The saturated hydraulic conductivity
251 is K_S = 8.16 m/day, the porosity (saturated water content) is θ_s = 0.287 and the residual water
252 content is θ_r = 0.075. The values of the soil properties used to parameterize the retention
253 curve (equation 8) are A = 1.61×10^6 and B = 3.96 and those for the relative conductivity
254 expression (equation 9) are C = 1.18×10^6 and D = 4.74.

255 4.1.2. Results and discussion

256 The domain of study is discretized in 71 nodes with a constant spacing of 0.01 m. Transient
257 simulations are performed during a period of 0.8 hours using a varying time step technique,
258 $\Delta t_0 = 0.1\times10^{-2}$ hr, $\Delta t_{min} = 0.1\times10^{-5}$ hr, $\Delta t_{max} = 0.1\times10^{-1}$ hr, $\Delta t_{mag} = 1.2$, $\Delta t_{red} = 0.5$, along with
259 $maxit_1 = 10$, $maxit_2 = 20$ and $maxit = 30$. A tolerance of $10^{-3}\,m$ is fixed for non linear
260 iterations. The linear system of equations is solved directly using tridiagonal algorithm.
261 Transient solutions are then computed at each 0.1 hours during a total time simulation of 0.8
262 hours, both with the present model and the standard one. Simulation details are summarized in
263 Table 1.

264 Simulated and measured water content are shown in Fig.1. The numerical water content
265 profiles are identical for the standard formulation and the new model. Both are in good
266 agreement with the experimental results. Numerically, the two models perform quiet similarly
267 as it can be seen in Table 1. For every time simulation, the time steps number, the nonlinear
268 iterations number, the CPU times are almost the same, as well as the mass balance error. The
269 new model (version M_1) performs similarly, but takes 2 or 3 iterations more to converge to
270 the same solution.

271 4.2. Two-dimensional, transient variably saturated water-table recharge

272 4.2.1. Description

273 This test case is taken from Vauclin et al. (1979) and involves a transient flow through a
274 homogeneous and isotropic rectangular soil embankment of 6.00 length and 2.00 m height.
275 The soil surface is recharged with a constant flux of q = 3.55 m/day, applied over a strip of
276 1.00 m width, located at the center of the domain. The remaining surface is covered to avoid
277 evaporation. Because of symmetry, only one part of the whole domain is to be modeled (for
278 instance, the right one). The subsequent domain is of 3.00 m by 2.00 m and the recharge flux

is then applied over a 0.5 m wide strip. The remaining soil surface is subject to no-flow condition as well as the bottom and the left side of the resulting domain. Fixed head boundary is used at the wetting zone of the right side of the domain by maintaining the water level at 0.65 m, whereas a no-flow condition is set to the remaining zone (Clement et al, 1994).

The soil properties are those of Vauclin et al. (1979). The saturated hydraulic conductivity is K_S = 8.40 m/day, the porosity (saturated water content) is θ_s = 0.30 and the residual water content is θ_r = 0.30. The values of the soil properties used to fit Van Genuchten's (1980) retention curve model (equations 4 and 5) are α = 3.3 m^{-1} and n = 4.1 (Clement et al, 1994; Kuznetsov et al, 2012). Specific storage is set to zero (Clement et al, 1994).

4.2.2. Results and discussion

Two grids are used, one coarse, with nodal distance of Δx = 0.1 m along the horizontal axis, and Δz = 0.05 m with respect to the vertical axis. For the fine grid, nodal distances are taken to be the half of those of the coarse grid. For the initial conditions, the water level is fixed to 0.65 m throughout the whole domain. Transient simulations are performed during a period of 8 hours using a varying time step technique, $\Delta t_0 = 0.1\times10^{-2}$ hr, $\Delta t_{min} = 0.1\times10^{-6}$ hr, Δt_{max} = 0.1 hr, Δt_{mag} = 1.2, Δt_{red} = 0.5, with $maxit_1$ = 10, $maxit_2$ = 10 and maxit = 30. A tolerance of $10^{-3}\,m$ is fixed for non linear iterations and 10^{-12} for inner ICCG iteration. Transient solutions are then computed at 2, 3, 4 and 8 hr elapsed time, using the present model and the standard one. Simulation details, related to the coarse grid, are exhibited in the Table 2.

Simulated water-table positions for different periods independently of the model are in good agreement with the measured data of Vauclin et al. (1979), as it can be seen in Fig.2. However, the solutions obtained with the fine grid are more close to the experimental data. The proposed model (M_1 and M_2) and the standard one provide identical solution. The two versions of the present model, in all cases, converge in less CPU time when compared to the

303 standard model. Overall, the standard model takes more CPU time to achieve the convergence
304 to the fixed level of accuracy. The best performance is recorded by the version M_2 of the
305 proposed model. As an example, during the 2 hours duration of the first period, the
306 convergence of the version M_2 is accomplished in 6401 iterations for 436 s whereas the
307 version M_1 converges in 9552 iterations for 617 s and the standard one converges in 7839
308 iterations for 993 s. However, on a per-non linear iteration basis, the versions M_1 and M_2 of
309 the present model and the standard one needed respectively an average CPU time of 0.0645 s,
310 0.0681 s and 0.1266 to converge. In addition, the version M_1, the standard model and, in a
311 lesser extent, the version M_2, experience difficulties during the iterative process which is
312 reflected by the number of the needing back steps, 6 for the version M_1, 5 for the standard
313 model and only 2 for the version M_2. The mass balance errors are of 0.215×10^{-1} % and
314 0.208×10^{-1} %, for the standard and the version M_2, respectively, and of 0.398 % for the
315 version M_1. The same performances of the competing models can be observed at the end of
316 the other periods of simulation. The overall CPU time required for the version M_2 to attain the
317 solution is about 2.3 times lesser than that needed by the standard model.

318 For the fine grid, the same outcome is observed regarding the rate of convergence and the
319 efficiency of the 3 models, with, however, the CPU time needed for model M_2 about 2.5 times
320 lesser than that necessitated by the standard model.

321 4.3.1. Description

322 This test deals with three-dimensional flow in an unsaturated porous media. The flow domain
323 is taken as a very dry cubic block of soil of length a = 15 m and is discretized with hexahedral
324 elements of size $0.25\times0.25\times0.25$ m^3. Because of the symmetry of the problem, only the half
325 of the domain is discretized, resulting in 58621 nodes and 54000 elements. On the top and the
326 bottom of the cubic domain, the pressure head is given by:

327 $\psi(x, y, z, t) = \frac{1}{\alpha}\ln\left(e^{\alpha\psi_r} + (1 - e^{\alpha\psi_r})\sin\frac{\pi x}{a}\sin\frac{\pi y}{a}\right)$ and $\psi = \psi_r$ respectively, where as a non-

328 flux condition is assigned to the vertical sides. To complete the problem the following initial

329 conditions are taken, $h(x, y, z, 0) = \psi_r + z$, where z indicates elevation. The relative

330 conductivity is modeled as $k_r = e^{\alpha\psi}$. and he moisture content as $\theta = \theta_r + (\theta_s - \theta_r)\, e^{\alpha\psi}$, where

331 θ_s is the saturated moisture content and θ_r is the residual content. Parameters of the problem

332 are : $\alpha = 0.25$, $\theta_s = 0.45$, $\theta_r = 0.15$, $\psi_r = -15$ m and the saturated hydraulic conductivity is

333 taken $K_s = 0.15$ m/day.

334 4.3.2. Results and discussion

335 Transient simulations are conducted during a period of 15 days using a varying time step

336 technique, $\Delta t_0 = 0.01$ day, $\Delta t_{min} = 0.001$ day, $\Delta t_{max} = 0.025$ day, with $maxit_1 = 10$, $maxit_2 = 10$

337 and maxit = 30. Transient solutions are then computed at 2.5, 5, 10, and 15 days elapsed time,

338 using the present model and the standard one. Simulation details are listed in Table 3.

339 Fig. 3 shows the pressure head contours at different times obtained with the present numerical

340 model (versions M_1 and M_2) and the standard one, together with those obtained with the

341 analytical solution (Tracy, 2006). Very good agreement can be noted between the solutions.

342 As for the precedent cases, the present model performs better than the standard one for all

343 time simulations. In addition, the version M_1 ensures its superiority when compared to the

344 version M_2. On a per-non linear iteration basis, for all the time simulations, the versions M_1

345 and M_2 of the present model needed an average of 8.23 s and 8.96 s of CPU time,

346 respectively, to converge, whereas an average time of 25.83 s is required for the standard

347 model, which represent more than 3 times the time needed by the present model, in the case

348 of the version M_1, and slightly less than 3 for the other version. Overall, with respect to the

349 total CPU time, the standard model takes about 3.11 times and 2.88 times the CPU time

needed for the versions M_1 and M_2, respectively, to converge. The standard model is very costly in terms of CPU time. As an example, during the 15 days period of simulation, the CPU time needed for the standard model to attain the solution is 9 hr 51 min 40 s, whereas 3 hr 10 min and 3 hr 25 min were recorded for the versions M_1 and M_2, respectively. Again the version M_1 of the presented model shows its highest efficiency.

Regarding the rate of convergence, the three models show practically the same number of iterations for every time simulation, despite a little advantage of the standard model and the version M_2 against the version M_1, which takes 7 more iterations to accomplish the convergence to the same solution. None of the 3 models had experienced difficulties to converge during all the periods of simulation, thus any back step was noticed. Finally, the Present model and the standard one show very satisfactory mass balance. The absolute values of the mass balance errors for almost all simulations are less than 10^{-3} %.

4.4. Three-dimensional transient variably saturated infiltration and pumping

4.4.1. Description

Two tests are involved and are taken from Kuznetzov et al. (2012), both deals with three-dimensional flow in a variably saturated porous media. Recharge from the top is considered first and pumping is studied afterwards, separately. The flow domain is a rectangular parallelepiped of 1000 m in both lateral directions and of 10 m height. The domain is discretized with hexahedral elements of size $10\times10\times1$ m^3 resulting in 112211 nodes and 100000 elements. For the infiltration case, the boundaries of the domain are subject to no flow condition except the top, which receives a recharging flux of 0.01 m /day from a square area of 100 m×100 m, located at the centre of the surface domain, whereas the remainder part is taken to be impervious. For the pumping case, the boundaries of the domain are subject to no flow condition and a fully penetrating vertical well is situated in the centre of the domain and

374 screened over 2 m from the bottom, with constant pumping rate 50 m^3/day, during 150 days.
375 For the both cases, the initial water table height is of 5 m from the bottom of the domain.
376 Parameters of the soil properties used along with the Van Genuchten's (1980) retention curve
377 model are $\alpha = 0.145$ m^{-1} and $n = 2.68$ (Kuznetsov et al, 2012) and the saturated hydraulic
378 conductivity is taken $K_s = 5$ m/day.

379 4.4.2. Results and discussion

380 Transient simulations are conducted during a period of 150 days using a varying time step
381 technique, $\Delta t_0 = 0.1$ day, $\Delta t_{min} = 0.001$ day, $\Delta t_{max} = 1$ day, with $maxit_1 = 10$, $maxit_2 = 10$ and
382 maxit = 30. A tolerance of $10^{-3}\,m$ is fixed for non linear iterations and 10^{-12} for inner PCG
383 iteration. Transient solutions are then computed at 50, 100, and 150 days elapsed time, using
384 the present model and the standard one. Tables 4 and 5 summarize simulation results and
385 simulated water-table positions obtained are shown in Fig.4.

386 As can be expected, the present model performs better than the standard one for all time
387 simulations. Also, the version M_1 shows again its relative superiority when compared to the
388 version M_2. On a per-non linear iteration basis, for all the time simulations, the versions M_1 of
389 the present model necessitated an average of 24.20 s to converge and the version M_2 needed
390 an average of 25.44 s of CPU time to achieve the convergence, while the standard model
391 required an average time of 93.24 s to accomplish the convergence to the same level of
392 accuracy. For the pumping case the performances are of 24.10 s, 25.39 s and 90.68 s of CPU
393 time, respectively. Consequently, the versions M_1 and M_2 of the present model are more than
394 3 times and half faster than the standard model. Globally, with respect to the total CPU time,
395 the standard model takes about 3.85 times and 3.66 times the CPU time needed, respectively,
396 for the versions M_1 and M_2 to converge when dealing with infiltration and about 3.95 times
397 and 3.74 times the CPU time needed in case of pumping. This demonstrates the high

computational cost of the standard model and the highest efficiency of the version M_1 of the present model.

Concerning the rate of convergence, the three models show exactly the same number of iterations for every time simulation. No resize was necessary for the time step already fixed, depending on the convergence history, during all the time simulations. Finally, the two versions of the present model show very satisfactory mass balance, contrarily to the standard model. Indeed, for all the simulations, the mass balance errors are under 10^{-2} % for the present model and are more than 5% for the standard model, in the infiltration case and are under 0.1 % for the present model and more than 10.0% for the standard model, when dealing with pumping.

As a comparison with an already published work, Kuznetzov et al. (2012) studied the same test (medium scale) and reported that their Quasi-3D model performs almost as a standard full-3D model. The CPU time needed for the standard full-3D is almost about 1.16 times superior to the CPU time needed for the Quasi-3D model.

4.5.1. Description

This example deals with a hypothetical large scale groundwater flow problem in a semi-arid context that is described by Prudic et al. (2004). The flow domain is a closed alluvial basin in which recharge is tributary to interactions between the aquifer and the rivers that cross it, broadly, from northwest to southeast and from east to west. The aquifer is constituted of unconsolidated deposits of mostly sand and gravel overlying a substratum that is many times less permeable than the filling material of the valley, which thickness increase toward the centre. A three dimensional structured mesh of this hypothetical aquifer is generated and adjusted to fit aquifer geometry and wells location. Maps of the aquifer top and bottom are presented in Fig.5 below. The studied domain is discretized into non uniform finite

422 hexahedral elements by a 51×54×11 mesh, respectively in x-, y- and z-direction, resulting in
423 30294 nodes and 26500 elements.

424 The boundaries of the domain are subject to no flow condition except the top where
425 evaporation occurs, mostly in the vicinity of the streams network, as described in Prudic et al.
426 (2004), when the depth of the free surface is less than a certain value (6.5 m for the present
427 simulations) and with variable rates, to a maximum of 0.0021 m/d. The streambed thickness is
428 of 0.915 m and the corresponding leakance is globally constant of 0.864 d^{-1}, but can reach
429 locally 1.728 d^{-1} in the blue river (Prudic et al, 2004). The elevation of the water in different
430 streams (sum of the streambed thickness and the stream depth) is taken constant and equal to
431 1.25 m.

432 For the retention curve model, Brooks and Corey's model (1964) is chosen (equations 6 and
433 7) with the sets of values of Herrada et al. (2014) and which are used as follows: in the
434 vicinity of the channels (θ_s = 0.396, θ_r = 0., ψ_s = –0.131 m and λ=0.127) and (θ_s = 0.477, θ_r =
435 0.1, ψ_s = –0.45 m and λ=1.20) for the sediments in the remainder part of the valley. The
436 hydraulic conductivity is taken as in Prudic et al. (2004): 52.8 m/d in the vicinity of the
437 streams and 10.7 m/d elsewhere. Ten pumping wells are considered; from each one, an
438 amount of 40000 m^3/d is extracted during a period of 50 years. The initial conditions are
439 provided as a result of a steady-state simulation of the model without pumping.

440 4.8.2. Results and discussion

441 Two simulations were conducted to provide the results presented in the framework of this
442 study. First, a steady-state simulation without pumping, but taking into account leakage and
443 evaporation, was conducted to provide initial conditions inputs necessary to the transient
444 simulation. For this purpose, a constant guess water head of 320.25 m was used for all the
445 nodes. A tolerance of 10^{-4}, using the relative norm, is fixed for non linear iterations together

with a tolerance of 10^{-12} for inner PCG iteration. The steady-state simulation, performed with the present model, required 18 iterations to converge to the specified criteria with an error mass balance of 0.211%. The CPU time needed for the model to converge in steady-state regime is 44.3 s. The standard model, however, fails to converge to the same level of solution mentioned above. The convergence of the standard method is also examined with alleviated criteria and did not converge even with non linear tolerance reduced to 10^{-2}. Indeed, the inner iterations (i, e), the PCG iterations, fail to converge when the inner tolerance is still 10^{-12}. With less drastic conditions (non linear tolerance of 10^{-2} and inner tolerance of 10^{-5}) the standard method reaches convergence in 17 iterations within 125 s of CPU time and with a mass balance error of 34.6%, whereas, the present new model converges in 2 iterations within only 11.8 s of CPU time and with a mass balance error of 0.866%. Fig.6 (left) shows steady-state water-table contours.

Transient simulations are conducted during a period of 50 years using a varying time step technique, Δt_0 = 15 day, Δt_{min} = 5 day, Δt_{max} = 365 day, with $maxit_1$ = 10, $maxit_2$ = 10 and maxit = 30. A tolerance of 10^{-4} is fixed for non linear iterations and 10^{-12} for inner PCG iteration. Transient solutions are then computed at 50 years elapsed time, using the present model and the standard one. Table 6 displays obtained simulation results.

Fig.6 (right) exhibits water level contours obtained with the version M_1 of the present model after 50 years of pumping.

For this mimicking real world groundwater flow problem, the present model shows its absolute superiority compared to the standard model. The versions M_1 and M_2 of the present model achieve the convergence in 167 and 301 iterations with CPU times, respectively, of 584 s and 1040 s, whereas, for the standard model, the convergence is achieved in 450 iterations within 5680 s. On a per-iteration basis, standard model, version M_1 and version M_2

of the present model need, respectively, 12.62 s, 3.45 sand 3.5 s CPU time. Thus, the present model (versions M_1 and M_2) is about 3.6 times faster than the standard one. In addition, regarding the total CPU time, the version M_1 of the present model is almost 10 times faster than the standard model and almost 2 times faster than the version M_2 of the present model, which demonstrates the high convergence rate of the version M_1 compared to the standard model and the version M_2 of the present model. This is confirmed by the iterations numbers needed for convergence which are of 167, 301 and 450, respectively for the versions M_1 and M_2 of the present model and the standard one. As it can be seen, particularly for this real world test, the version M_1 of the present model shows the highest numerical efficiency to solve large and complex groundwater flow problems.

Regarding the mass balance analysis, the versions M_1 and M_2 provide satisfactory mass balance, 0.144% and -0.633%, contrarily to the standard model which shows an excessively high mass balance error of 131%. Thus, the standard model (equations 12 and 14) may be inadequate to solve complex groundwater flow problems, in addition to its high numerical cost. Fig.7 shows the solutions obtained with the version M_1 and M_2 of the present model together with the solution obtained with the standard one.

5. Conclusions

An efficient transient numerical mass-conservative model is constructed to solve variably saturated groundwater flow problems. A Galerkin linear finite element mesh is used to discretize the entire domain, saturated and unsaturated compartments. Picard iteration technique, together with the fully implicit Euler method, is used to solve the obtained discretized equations system. The present model is particularly suitable for limited computational resources when 3D groundwater flow problems are tackled. The stiffness and mass matrices involved are approximated in a way that only hydraulic properties are updated during the iterative process to guarantee less computational effort, when solving the PDE. The

495 geometric part of the matrices remains unchanged, so computed once and stored, which
496 ensures important savings in CPU time. The new model is presented with or without
497 approximate mass matrix (versions M_1 and M_2). Both are tested and compared to a standard
498 numerical model obtained with non altered matrices.

499 The proposed model capabilities are tested and compared to the standard model across
500 benchmark tests for which analytical solutions or experimental results are available. A "real
501 world" groundwater flow problem is also solved to examine the performance of the
502 competing numerical tools. Different soil water curve models, conferring variable non
503 linearity degrees to the Richards equation, are also implemented. Emphasis is made when
504 reproducing these examples on two major aspects, that are accuracy and efficiency assessed,
505 respectively, by the mass balance error and the CPU time to achieve convergence.

506 Along with the studied examples, the developed new model shows its superiority to solve
507 variably saturated flow problems in 1D, 2D and 3D configurations. The developed new model
508 exhibits high computational performance regarding time cost and solution accuracy. These
509 outcomes are clearly revealed with high dimensionality problems. In effect, the present model
510 and the standard one perform almost similarly when dealing with 1D flow problems, may be,
511 because of the relatively small number of nodes and elements. The numerical water content
512 curves are identical and the CPU times are very close as well as the mass balance errors.
513 Since the dimensionality increases, the present model (M_1 and M_2) performs increasingly
514 better than the standard model. The latter is computationally intensive due to the fact that the
515 involved matrices should be, totally rebuilt, at every nonlinear iteration, contrarily to the
516 proposed new model, where only the hydraulic parts are to be updated; the geometric parts are
517 computed once and stored. As a consequence, the CPU time needed to attain the convergence
518 becomes dramatically highest for the standard model. It is clear that the required CPU time
519 increases with high dimensionality and the total number of elements and nodes.

For the 2D recharge test, the CPU time needed by the standard model is about 2.3–2.5 times higher than the CPU time needed for the present model, whereas the mass balance errors are satisfactory for the competing models. When dealing with the 3D flow examples the CPU time needed by the standard model to achieve convergence is about 3.66–3.95 times greater than that needed by the present model to converge to the same level of accuracy. On the other hand, the mass balance error is very satisfactory for the present model, less than 0.01% for the recharge test and less than 0.1% for test of pumping, whereas for the standard model, these mass balance errors are more than 5% and more than 10% for the two tests mentioned, respectively. It is to notice that the mass balance error provided by the two competing model are very satisfactory (less than 0.001%), when dealing with the totally unsaturated flow example. Indeed, the numerical solutions obtained with the two models (present and standard) match very well. However, the CPU time needed by the standard model to converge under the same constraints is globally about 3 times greater than that needed for the present model.

For the hypothetical real word test, the present model shows its absolute superiority when compared to the standard model. Also, the version M_1 confirms its superiority when compared to the version M_2. Globally, with respect to CPU time, the standard model takes almost 10 times and more than 5 times the CPU time needed respectively by the versions M_1 and M_2 of the present model to converge. This, clearly, shows the highest efficiency of the version M_1 of the present model. The version M_2 take about 2 times the CPU time needed to the version M_1 to converge, indeed. Regarding the mass balance analysis, the versions M_1 and M_2 provide satisfactory mass balance, 0.144% and -0.633%, contrarily to the standard model which shows an excessively high mass balance error of 131%.

As it can be seen, particularly for this real world test, the version M_1 of the present model shows the highest numerical efficiency to solve large and complex groundwater flow problems. Consequently, the use of the standard model to solve groundwater flow problems

may be difficult and almost prohibitive to perform more complicated and repetitive operations as the calibration, for instance, or to solve coupled groundwater flow and solute transport problems, particularly with poor or insufficient computational resources. The present model, however, particularly the version M_1, is shown to be suitable for solving large and complex groundwater flow problems and, probably, to be used usefully for the anticipated related issues.

References

Aharmouch, A., Amaziane, B., 2012. Development and evaluation of a numerical model for steady state interface and/or free surface groundwater flow. J. Hydrol. 434-435, 110-120.

Belfort, B., Younes, A., Fahs, M., Lehman, F., 2013. On equivalent hydraulic conductivity for oscillation-free solutions of Richards equation. J. Hydrol. 505, 202-217.

Brooks, R.H., Corey, A.T., 1964. Hydraulic properties of porous media. Hydrol Pap. 3. Colorado State Univesity, Fort Collins, Colorado.

Celia, M.A., Boulotas, E.T., Zarba, R.L., 1990. A general mass-conservative numerical solution for the unsaturated flow equation. Water Resour Res. 26, 1483-1496.

Clement, T.P., Wise, W.R., Molz, F.J., 1994. A physically based, two-dimensional, finite-difference algorithm for modeling variable saturated flow. J. Hydrol. 161, 71-90.

Fahs, M., Younes, A., Lehmann, F., 2009. An easy and efficient combination of the Mixed Finite Element Method and the Method of Lines for the resolution of Richards' Equation. Environ. Modell. Softw. 24, 1122-1126. https://doi.org/10.1016/j.envsoft.2009.02.010 .

Farthing, M.W., Ogden, F.L., 2017. Numerical Solution of Richards' equation: a review of advances and challenges. Soil Sci. Soc. Am. J. 81, 1257-1269. https://doi.org/10.2136/sssaj2017.02.0058

568 Gardner, W. R., 1958. Some steady-state solutions of the unsaturated moisture flow equation
569 with application to evaporation from a water table. Soil Sc., 85, 228-232.

570 Hassane Maina, F., Ackerer, P., 2017. Ross scheme, Newton-Raphson iterative methods and
571 time-stepping strategies for solving the mixed form of Richards' equation. Hydrol. Earth Syst.
572 Sci. 21, 2667-2683. https://doi.org/10.5194/hess-21-2667-2017

573 Moutsopoulos, K. N., 2013. Solutions of the Boussinesq equation subject to a nonlinear Robin
574 boundary condition. Water Resour. Res. 49, doi:10.1029/2012WR012221.

575 Haverkamp, R., Vauclin, M., Touma, J., Wierenga, P.J., Vachaud, G., 1977. Comparison of
576 numerical simulation models for one-dimensional infiltration. Soil Sci. Am. J. 41, 285-294.

577 Hayek, M., 2015. An analytical model for steady vertical flux through unsaturated soils with
578 specific hydraulic properties. J. Hydrol. 527, 1153-1160.

579 Herrada, M.A., Gutierrez-Martin, A., Montanero, J.M., 2014. Modeling infiltration rates in
580 saturated/unsaturated soil under the free draining condition. J. Hydrol. 515, 10-15.

581 Irmay, S.,1954. On the hydraulic conductivity of unsaturated soils, Eos Trans. AGU. 35, 463-
582 467.

583 Kuznetsov, M., Yakirevich, A., Pachepsky, Y.A., Sorek, S., Weisbrod, N., 2012. Quasi 3D
584 modeling of water flow in vadose zone and groundwater. J. Hydrol. 450-451, 140-149.

585 Koohbor et al. (2021) An advanced discrete fracture model for variably saturated flow in
586 fractured porous media, https://doi.org/10.1016/j.advwatres.2020.103602

587 Paniconi, C., Putti, M., 1994. A comparison of Picard and Newton iteration in the numerical
588 solution of multidimensional variably saturated flow problems, Water Resour Res. 30(12),
589 3357-3374.

590 Paulus, R., Dewals, B.J., Erpicum, S., Pirotton, M., 2013. Innovative modelling of 3D
591 unsaturated flow in porous media by coupling independent models for vertical and lateral
592 flows. J. Comput. Appl. Math. 246, 38-51.

593 Polubarinova-Kochina, P. Y., 1962. Theory of groundwater movement. Translated from
594 Russian by J. N. R. de Wiest. Princeton University Press. Princeton. N. J.

595 Prudic, D.E., Konikow, L.F., Banta, E.R., 2004. A new Stream-Flow Routing (SFR1) package
596 to simulate stream–aquifer interaction with MODFLOW2000. Open-File Rep. 2004-1042.
597 USGS, Carson City, NV.

598 Šimůnek, J., van Genuchten, M.Th., Šejna, M., 2006. The Hydrus software pachage for
599 simulating two- and three-dimensional movement of water, heat and multiple solutes in
600 variably saturated media. Technical manual, version 1.0, PC Progress, Prague, Czeck
601 Republic.

602 Thoms, R.B., Johnson, R.L., Healy, R.W., 2006. User's guide to the variably saturated flow
603 (VSF) process for MODFLOW; technique and Methods 6-A18. USGS, Reston, VA.
604 http://pubs.usgs.gov/tm/2006/tm6a18/ (verified 13.05.09.).

605 Teloglou, I.S, Zissis, T.S., Panagoupolos, A.C, 2008. A water table fluctuation in aquifers
606 overlying a semi-impervious layer due to transient recharge from a circular basin. J. Hydrol.
607 348, 215-223.

608 Tracy, F. T., 1995. 1-D, 2-D, and 3-D analytical solutions of unsaturated flow in groundwater.
609 J. Hydrol. 170, 199-214.

610 Tracy, F. T., 2006. Clean two- and three-dimensional analytical solutions of Richards'
611 equation for testing numerical solvers. Water Resour. Res. 42, W08503,
612 doi:10.1029/2005WR004638.

613 Tracy, F. T., 2007. Three-dimensional analytical solutions of Richards equation for a box-

614 shaped soil sample with piecewise-constant head boundary conditions on the top. J. Hydrol.
615 336, 391-400.

616 Twarakavi, N.K.C., Šimůnek, J., Seo, S., 2008; Evaluating interactions between groundwater
617 and vadose zone using the HYDRUS-based flow package for MODFLOW. Vadose Zone J. 7,
618 757-768.

619 Van Dam, J.C., Feddes, R.A., 2000. Numerical simulation of infiltration, evaporation and
620 shallow groundwater levels with the Richards equation. J. Hydrol. 233, 72-85.

621 Van Genuchten, M. Th.,1980. A closed-form equation for predicting the hydraulic conductivity of
622 unsaturated soils. Soil Sci. Soc. Am. J. 44, 892-899.

623 Vauclin, M., Khanji, D., Vachaud, G., 1979. Experimental and numerical study of a transient,
624 two-dimensional unsaturated-saturated water table recharge problem. Water Resour. Res.
625 15(5), 1089-1101.

626 Xu, X., Huang, G., Zhan, H., Qu, Z., Huang, Q., 2012. Integration of SWAP and
627 MODFLOW-2000 for modeling groundwater dynamics in shallow water table areas. J.
628 Hydrol. 412-413, 170-181.

629 Yakirevich, A., Borisov, V., Sorek, S., 1998. A quasi three-dimesional model for flow and
630 transport in unsaturated and saturated zones: 1. Implementation of the quasi two-dimensional
631 case. Adv. Water Resour. 21(8), 679-689.

632 Yeh, G. T.,1981. On the computation of darcian velocity and mass balance in the finite element
633 modeling of groundwater flow. Water Resour. Res. 17, 1529-1534.

634 Younes, A., Fahs, M., Belfort, B., 2013. Monotonicity of the cell-centred triangular MPFA
635 method for saturated and unsaturated flow in heterogeneous porous media. J. Hydrol. 504,
636 132-141.https://doi.org/10.1016/j.jhydrol.2013.09.041 .

637 Zha, Y., Yang, J., Yin, L., Zhang, Y., Zeng, W., Shi, L., 2017. A modified Picard iteration

638 scheme for overcoming numerical difficulties of simulating infiltration into dry soil. J.
639 Hydrol. 551, 56-69.

640 Zha, Y., Yang, J., Zeng, J., Tso, C.M., Zeng, W., Shi, L., 2019. Review of numerical solution
641 of Richardson-Richards equation for variably saturated flow in soils. WIREs Water
642 6.https://doi.org/10.1002/wat2.1364 .

643

644

645

646

647

648

649

650

651

652

653

654

655

656

657 Table 1. Simulation results for the transient flow in a soil column under infiltration

Model	Δz	Time	Nts	Nbs	CPU	Nnlit	MBE (%)

	(m)	(hr)			(s)		
New, M_2	0.01	0.1	19	0	2.31	82	-0.261E-3
Stand	0.01	0.1	19	0	2.36	82	-0.165E-3
New, M_2	0.01	0.2	29	0	3.52	126	0.583E-3
Stand	0.01	0.2	29	0	3.51	126	0.927E-3
New, M_2	0.01	0.3	39	0	4.56	166	0.103E-2
Stand	0.01	0.3	39	0	4.62	166	0.162E-2
New, M_2	0.01	0.4	49	0	5.66	206	0.940E-3
Stand	0.01	0.4	49	0	5.72	206	0.192E-2
New, M_2	0.01	0.5	59	0	6.70	246	0.912E-3
Stand	0.01	0.5	59	0	6.76	246	0.212E-2
New, M_2	0.01	0.6	69	0	7.80	286	0.924E-3
Stand	0.01	0.6	69	0	7.85	286	0.224E-2
New, M_2	0.01	0.7	79	0	8.84	326	0.894E-3
Stand	0.01	0.7	79	0	8.96	326	0.228E-2
New, M_2	0.01	0.8	89	0	9.94	366	0.525E-3
Stand	0.01	0.8	89	0	10	366	0.204E-2

658

659

660

661

662

663

664 Table 2. Simulation results for the transient two-dimensional water-table recharge

Model	Δx	Δz	Time	Nts	Nbs	CPU	Nnlit	MBE (%)

	(m)	(m)	(hr)			(s)		
New, M_1	0.1	0.05	2	779	6	617	9552	0.398
New, M_2	0.1	0.05	2	541	2	436	6401	0.208E-1
Stand	0.1	0.05	2	685	5	993	7839	0.215E-1
New, M_1	0.1	0.05	3	810	6	636	9873	0.287
New, M_2	0.1	0.05	3	555	2	445	6540	0.142E-1
Stand	0.1	0.05	3	707	5	1020	8061	0.201E-1
New, M_1	0.1	0.05	4	834	6	651	10106	0.240
New, M_2	0.1	0.05	4	565	2	453	6636	0.111E-1
Stand	0.1	0.05	4	718	5	1030	8170	0.201E-1
New, M_1	0.1	0.05	8	875	6	676	10478	0.186
New, M_2	0.1	0.05	8	605	2	473	6937	0.622E-2
Stand	0.1	0.05	8	758	5	1080	8517	0.350E-1

Table 3. Simulation results for the transient, three-dimensional unsaturated flow

Model	Δx (m)	Δy (m)	Δz (m)	Time (days)	Nts	Nbs	CPU (s)	Nnlit	MBE (%)
New, M_1	0.25	0.25	0.25	2.5	103	0	2660	352	-0.232E-3
New, M_2	0.25	0.25	0.25	2.5	103	0	2850	345	-0.210E-3
Stand	0.25	0.25	0.25	2.5	103	0	8150	345	-0.449E-3
New, M_1	0.25	0.25	0.25	5	203	0	4420	552	-0.867E-3
New, M_2	0.25	0.25	0.25	5	203	0	4790	545	-0.106E-2
Stand	0.25	0.25	0.25	5	203	0	13600	545	-0.159E-2
New, M_1	0.25	0.25	0.25	10	403	0	7930	952	-0.444E-3
New, M_2	0.25	0.25	0.25	10	403	0	8570	945	-0.660E-3
Stand	0.25	0.25	0.25	10	403	0	24600	945	-0174E-2
New, M_1	0.25	0.25	0.25	15	603	0	11400	1352	-0.231E-3
New, M_2	0.25	0.25	0.25	15	603	0	12300	1345	-0.401E-3
Stand	0.25	0.25	0.25	15	603	0	35800	1345	-0.200E-2

686 Table 4. Simulation results for the transient, three-dimensional water-table recharge.

Model	Δx (m)	Δy (m)	Δz (m)	Time (days)	Nts	Nbs	CPU (s)	Nnlit	MBE (%)
New, M_1	10.0	10.0	1.0	50	59	0	2860	117	0.880E-2
New, M_2	100	10.0	1.0	50	59	0	3010	117	0.470E-2
Stand	10.0	10.0	1.0	50	59	0	10600	117	5.40
New, M_1	10.0	10.0	1.0	100	109	0	5310	217	0.508E-2
New, M_2	10.0	10.0	1.0	100	109	0	5530	217	0.403E-2
Stand	10.0	10.0	1.0	100	109	0	19500	217	5.46
New, M_1	10.0	10.0	1.0	150	159	0	7580	317	0.385E-2
New, M_2	10.0	10.0	1.0	150	159	0	8020	317	0.374E-2
Stand	10.0	10.0	1.0	150	159	0	30600	317	5.53

687

688

689

690

691

692

693

694

695

696

697

698

699

Table 5. Simulation results for the transient, three-dimensional water-table with pumping.

Model	Δx (m)	Δy (m)	Δz (m)	Time (days)	Nts	Nbs	CPU (s)	Nnlit	MBE (%)
New, M_1	10.0	10.0	1.0	50	59	0	3060	130	-0.255E-1
New, M_2	10.0	10.0	1.0	50	59	0	3230	131	-0.237E-1
Stand	10.0	10.0	1.0	50	59	0	12500	132	-12.8
New, M_1	10.0	10.0	1.0	100	109	0	5440	230	-0.291E-1
New, M_2	10.0	10.0	1.0	100	109	0	5750	231	-0.323E-1
Stand	10.0	10.0	1.0	100	109	0	20700	232	-12.8
New, M_1	10.0	10.0	1.0	150	159	0	7360	298	-0.265E-1
New, M_2	10.0	10.0	1.0	150	159	0	7780	298	-0.343E-1
Stand	10.0	10.0	1.0	150	159	0	29100	323	-12.7

714

715 Table 6. Simulation results for the transient, hypothetical river-connected aquifer.

Model	Δx (m)	Δy (m)	Δz (m)	Time (years)	Nts	Nbs	CPU (s)	Nnlit	MBE (%)
New, M_1	-	-	-	50	64	0	584	167	0.144
New, M_2	-	-	-	50	70	0	1040	301	-0.633
Stand	-	-	-	50	84	7	5680	450	131

716

717

718

719

720

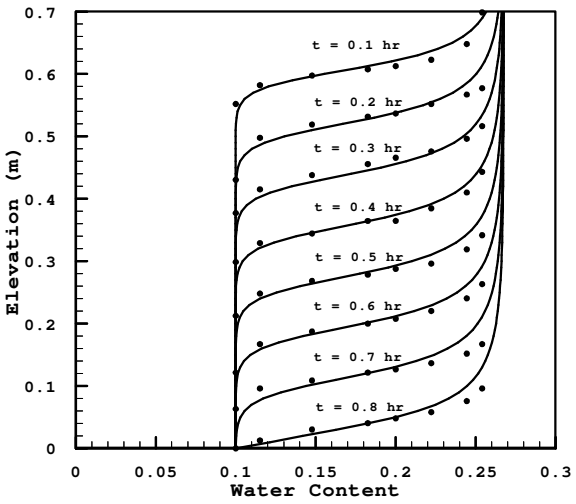
Elevation (m)
Water Content
0
0.1
0.2
0.3
0.4
0.5
0.6
0.7
0.05
0.15
0.25
t = 0.1 hr
t = 0.2 hr
t = 0.3 hr
t = 0.4 hr
t = 0.5 hr
t = 0.6 hr
t = 0.7 hr
t = 0.8 hr

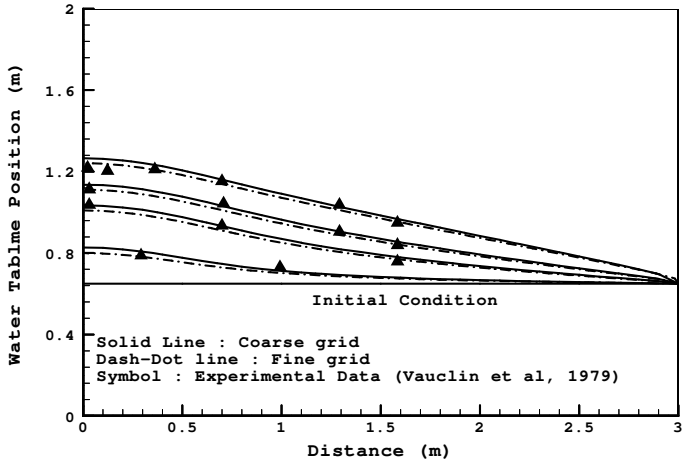
Water Tablme Position (m)
Distance (m)
Initial Condition
Solid Line : Coarse grid
Dash-Dot line : Fine grid
Symbol : Experimental Data (Vauclin et al, 1979)
0
0.4
0.8
1.2
1.6
2
0
0.5
1
1.5
2
2.5
3

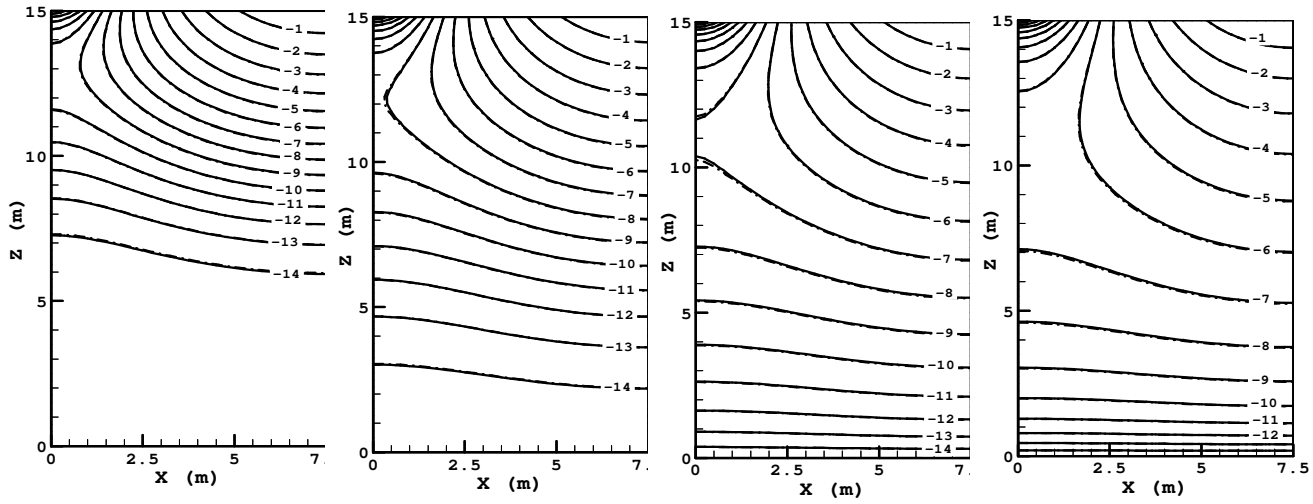
15
10
5
0
z (m)
X (m)
0
2.5
5
7.5
-1
-2
-3
-4
-5
-6
-7
-8
-9
-10
-11
-12
-13
-14

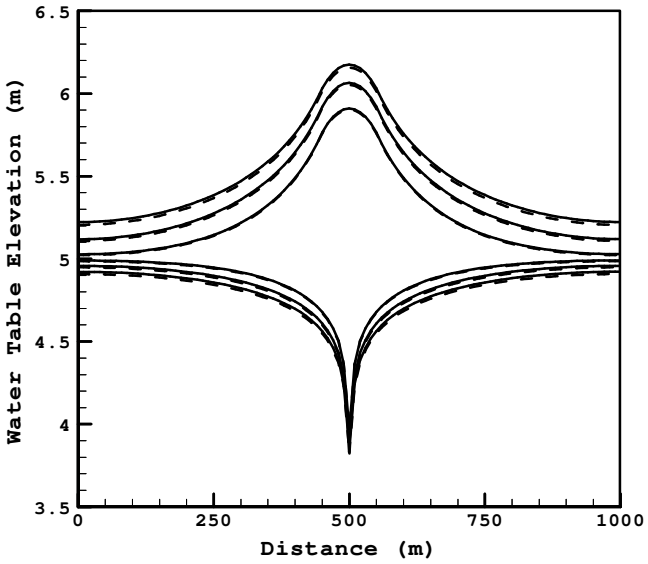
Water Table Elevation (m)
6.5
6
5.5
5
4.5
4
3.5
0
250
500
750
1000
Distance (m)

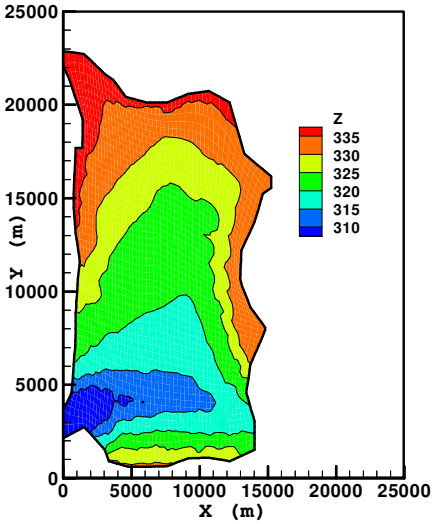
25000
20000
15000
10000
5000
0
Y (m)
0
5000
10000
15000
20000
25000
X (m)
Z
335
330
325
320
315
310

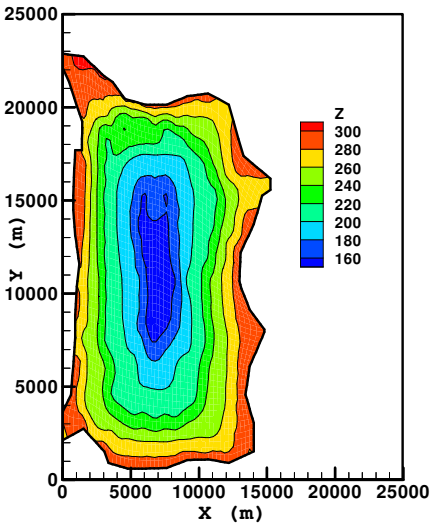
25000
20000
15000
10000
5000
0
Y (m)
0
5000
10000
15000
20000
25000
X (m)
Z
300
280
260
240
220
200
180
160

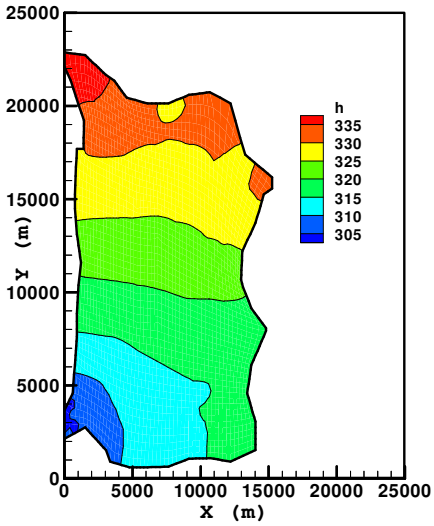
25000
20000
15000
10000
5000
0
Y (m)
0
5000
10000
15000
20000
25000
X (m)
h
335
330
325
320
315
310
305

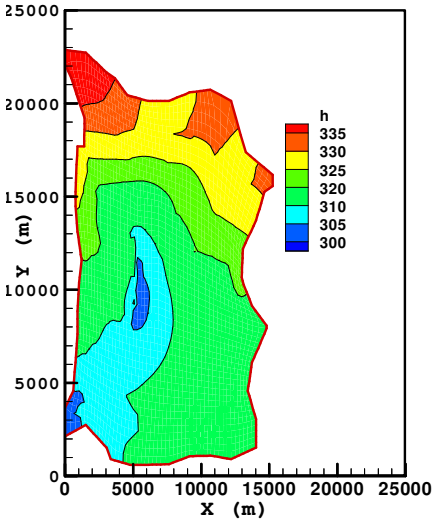
25000
20000
15000
10000
5000
0
Y (m)
0
5000
10000
15000
20000
25000
X (m)
h
335
330
325
320
310
305
300

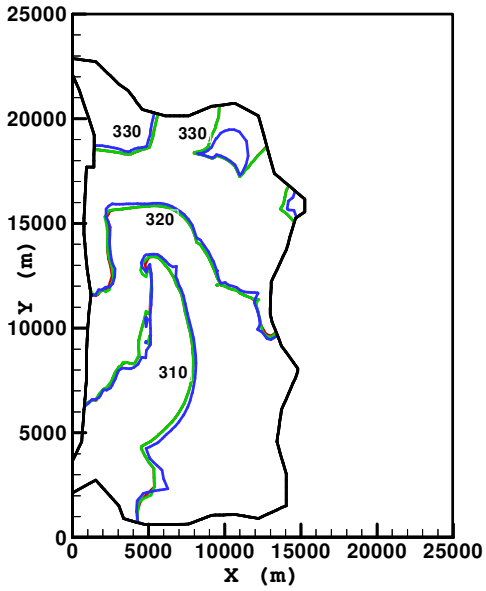
25000
20000
15000
10000
5000
0
Y (m)
330
330
320
310
0
5000
10000
15000
20000
25000
X (m)